Impact of the jet velocity on the turbulent liquid jet

Muhamad Said[1,*], Abouelmagd Abdelsamie[1], Kareem Emara[1], Momtaz Sedrak[1]

[1]Mechanical Power Engineering Department, Faculty of Engineering at Elmataria, Helwan University, Cario, Egypt.
[*]Corresponding author's e-mail: muhamad.said@m-eng.helwan.edu.eg

Abstract

This numerical study aims to investigate the impact of jet velocity and nozzle diameter on liquid turbulent jet. Incompressible large eddy simulations (LES) with Wall-Adapting Local Eddy-Viscosity (WALE) sub-grid scale model in ANSYS-FLUENT were performed to capture the morphology of the breakup as well as the important flow field characteristics. A volume of fluid (VOF) approach was used to track the unsteady evolution and breakup of the liquid jet. Different results have been analyzed to assess this impact. These results are instantaneous and time-averaged axial velocity, liquid volume fraction, and turbulent kinetic energy. The results are represented in contours and centerline- and radial-profiles. The surrounding gas density is 34.5 kg/m^3. The nozzle exit diameter is 0.05 mm. Three jet exit-velocities of 50 m/s, 100 m/s and 150 m/s are considered. The results showed that the predicted location, where drops and ligaments are first seen, moves away from the nozzle as the jet velocity increases, where this location was computed as $x = 3.5D, 6.5D$ and $7.5D$ for Case50, Case100 and Case150, respectively. Also, the predicted location, where surface waves developed from Kelvin-Helmholtz instability are first seen, moves towards the nozzle as the jet velocity increases, where this location was computed as $x = 1.6D, 1D$ and $0.5D$ for Case50, Case100 and Case150, respectively. Regarding the jet dispersion angle and the liquid core length, it was found that they increase with increasing the jet exit velocity.

Keywords : Breakup, Turbulent jet, Large eddy simulation (LES), Jet dispersion angle.

Abbreviations:

ALVF	Average liquid volume fraction
CFL	Courant–Friedrichs–Lewy condition
DNS	Direct numerical simulation
LES	Large eddy simulation
LVF	Liquid volume fraction
RANS	Reynold-averaged Navier-Stokes
SGS	Sub-grid scale
SMD	Sauter mean diameter
TKE	Turbulent kinetic energy
VOF	Volume of fluid
WALE	Wall-Adapting Local Eddy-Viscosity

1. Introduction

Characterization of turbulent liquid jet exits of a simple orifice is particularly important in engineering because of its wide range of applications, such as: combustion, thermal spray, agriculture, inkjet, coating, medical sprays and much more [1]. Involvement of spray into many applications makes its study very important. Studying the spray enables us to control its characteristics. The importance of controlling the spray characteristics stems from the different characteristics needed by each application. Also, Studying the spray characteristics is a basic concept for development of the physical modeling tools that predict it. The process of turning the liquid jets into droplets, which is called disintegration, increases the liquid surface area, and thus increases the transfer of both mass and heat between the liquid and the surrounding fluid. Here, lies the importance of spray in the different applications [2]. Atomization study is undoubtedly fundamentally important process, and at the same time is very difficult and challenging because it is unsteady and complex behavior, and this is due to its involvement of different types of instabilities [3], [4].

Over the past years, many researchers devoted their efforts in describing the behavior of cylindrical liquid jets discharging into a quiescent gaseous atmosphere. The first experimental investigation was recorded in the first half of the nineteenth century [5]. When liquid is discharging from a circular opening, it is producing a cylindrical jet. The liquid discharging rate from the orifice is a key factor in the mechanisms of disintegration. The plot of the jet breakup length as a function of the orifice bulk exit velocity, which called stability curve, is the common way of categorizing the disintegration mechanisms of cylindrical jets [6], [7], [8], [9]. Breakup length is the coherent part of the jet, i.e., it is the length of the continuous jet connected to the nozzle [10].

Hiroyasu and Kadota [11] deduced an experimental relationship between pressure of the fuel injection, the density of ambient air, the mass flow ate of the fuel and the droplets Sauter mean diameter (SMD). Elkotb [12], Varde et al. [13] and Faeth et al. [14], studied additionally the effects of the density and viscosity of the liquid and the surface tension, where they deduced an experimental relationship between them and the droplets Sauter mean diameter (SMD). Moreover, an empirical relationship of breakup length of the liquid core was derived by Reitz and Bracco [15]. Implosion of cavitation bubbles, turbulence in the liquid jet and aerodynamic liquid-gas interaction were identified by Fath et al. [16] as the most dominant liquid jet atomization mechanism.

Gupta et al. [17] studied experimentally the primary atomization of evaporating laminar liquid jets of *n*-pentane and *n*-heptane emerging from a circular nozzle into high-temperature turbulent coflows of air in confined pipe. Their results in the near-field region of the injector nozzle showed that the length of the liquid jets formed increases with the fuel injection velocity and decreases with the air velocity. They also found that the smaller droplets were formed at higher

velocities of fuel and air. Furthermore, they observed, within their investigated range of conditions, that the jet length and droplet size are not affected by the air inlet temperature.

The atomization effect on entrainment in the gas phase of a 2-phase free jet, as a function of the mixing ratio, was investigated by Hotz et al. [18] at ambient conditions. They used the tracer gas (helium) concentration in the gas phase to indicate the local mixing ratios for 3 different nozzles by applying 5 different gas-to-liquid ratios (GLR) for the 2-phase free jet as well as a single-phase free jet.

The liquid preheating impact on primary jet breakup in a coaxial twin-fluid injector was investigated by Kumar and Sahu [19]. Recorded shadow-graphic images of 3 different jets, with different injection temperatures, taken by high speed camera were analyzed to measure several parameters such as the jet breakup length. It was found that preheating the jet to a medium temperature has a very strong effect on the breakup process of the jet.

As the mechanisms of cavitation bubbles implosion and liquid jet turbulence were related to phenomena inside the nozzle, many researchers studied the extent to which the breakup length of the liquid jet was affected by the flow inside the nozzle. For example, Martínez-Martínez et al. [20] concluded that, the nozzle diameter is a crucial factor affecting the penetration length. Furthermore, Suh and Lee [21] concluded that the fuel atomization and the cavitation bubble generation in the nozzle could be enhanced by increasing the ratio of the length of the nozzle to its width. Sirignano and Mehring [22] summarized a lot of previous works that considered the impact of liquid jet disintegration on the main flow fields.

When focusing carefully on aforementioned literature, one can notice that the process of atomization has been ignored, especially the part of primary step due to the diagnostic limitations. Later on, some diagnostics were developed to obtain more details by experiments. These diagnostics were mentioned in Refs. [23], [24], [25]. Following this development and other, rapid changes occurred in recent decades concurrently with the emergence of new experimental technologies. We should take advantage of this development in making more effort to study and investigate the part that was neglected in the past, i.e., the primary step of the atomization process, which is the main link between the liquid jet discharging from the nozzle and the fully developed spray [10], [26].

From the numerical point of view, over the years, huge efforts were made to simulate the breakup process of a liquid jet with several methods. These numerical studies were mainly based on solving Navier-Stokes equation which was accompanied by appropriate interface capturing method such as volume of fluid (VOF) [27], level set method [28] or a combination of both [29], [30]. Selection of the appropriate numerical method depends on the advantages and disadvantages of each method for each application separately, and it varies from one problem to another.

Among these numerical studies, research focused on the effect of the flow inside the nozzle on the breakup process of the jet. To name a few, Som et al. [31] solved the Reynolds-Averaged Navier–Stokes (RANS) equations to simulate the nozzle flow only. They analyzed the mass flow at the exit orifice of the nozzle as a function of injection pressure, the position of the needle left and the fuel type. Yuan and Schnerr [32] conducted RANS simulations to combine the in-nozzle flow with the discharged liquid jet. They studied two jet atomization cases, one of them include the cavitation phenomenon while the other was without the cavitation for the purpose of comparing the two cases for enhancing the atomization process.

Furthermore, Ghiji et al. [33] applies LES for in-nozzle flow and the following atomization, using simplifying nozzle. They found compatible results with that obtained experimentally during the Diesel injection initial stages. Xiao et al. [34] simulated the jet flow approach without the flow inside the nozzle. On the other hand, the evaluation of the in-nozzle swirl effect on the flow field of annular gas-liquid jets was studied by Siamas et al. [35] using detailed VOF simulations. They reported that central recirculation region was developed as a result of the swirling motion. Grosshans et al. [36] showed that the range of liquid-gas density ratio from 10 to 30 has a small effect on the aerodynamic breakup. Also, they reported that if the liquid gas viscosity ratio was reduced from 7 to 1, then the droplet becomes smaller and thus the dispersion angle becomes larger.

Shinjo and Umemura [37] discussed the physical mechanisms including ligament and droplet formation that still need further investigations, where they studied the primary atomization of liquid injected at high speed into still air to elucidate physical processes by direct numerical simulation (DNS).

Zhang *et al.* [38] studied the effect of the angle between the central liquid (glycerol/water mixture with a high dynamic viscosity of 200 mPa.s) jet and the annular airflow on the primary atomization process of coaxial, twin-fluid nozzle. They observed that increasing the angle from 0 to 30 ° promotes the breakup of the jet, increases the flow velocity of the gas phase close to the liquid jet and decreases its core length. However, further increase of the angle from 30 to 60 ° leads to a decreased gas flow velocity along the liquid jet and an increase of core length.

In an unconventional work, Leng *et al.* [39] simulated, using (VOF-LES) method, the multi-phase flow inside and outside the spirally grooved hole (SGH) nozzle to investigate its influence on the behavior of breakup process and cavitating flow characteristics for diesel nozzles. They found that the inner-hole's spiral grooves added more dynamics besides aerodynamic effects for the breakup of liquid jets which in turn led to strong enhancement of the emerging jet breakup and substantially near-field dispersion angle

Recently, Abdelsamie and Thévenin [40] , by means of DNS, quantified the impact of shear on evaporation and spray autoignition mechanisms by comparing droplets evolving in a high-speed jet flow or in a nearly quiescent environment. Also, the impact of local equivalence ratio, droplet

diameter and jet velocity were investigated by varying these parameters. They revealed in their results that the temporally-evolving jet is a promising numerical configuration to study spray-turbulence interaction, evaporation, mixing, and auto-ignition mechanisms.

From the literature reviewed in the previous paragraphs, it can be concluded that the most important parameters to be studied in the liquid turbulent jet are, the jet velocity, nozzle diameter, and the liquid-to-gas density ratio.

From the above-mentioned survey, plenty of literature investigated the impact of the mentioned parameters on the liquid jet but, there are several ranges, to the author knowledge, are still not yet covered. The present study tries to cover the missing ranges. Therefore, in this article, the impact of surrounding gas density on 0.2 mm diameter liquid turbulent jet was investigated. Incompressible-LES Simulations [41] with WALE sub-grid scale model [42] in ANSYS-FLUENT were performed to capture the morphology of the breakup as well as the important characteristics of the flow field. A volume of fluid (VOF) approach [27] was used to track the unsteady evolution and breakup of the liquid jet. For ambient gas density of 34.5 kg/m^3, three different jet exit-velocity of 50 m/s, 100 m/s and 150 m/s were considered.

This article organized as follows: the employed mathematical models are reviewed in Sec. 2, includes the applied LES method and the VOF model. The employed geometry, meshing, boundary conditions, and solvers will be discussed in detail in Sec. 3. At the end of Sec. 3, mesh dependency test and validation of turbulence and multiphase models will be introduced. The results of the investigation of the impact of the changing of gas density on the turbulent jet behavior will be discussed in Sec. 4. At the end, conclusions will be provided in Sec. 5.

2. Mathematical Models

In this section, the employed governing equations will be briefly summarized. In the first part, the applied LES method will be explained, while in the second one, the VOF model will be presented.

2.1. LES-WALE Model

Large eddy simulation (LES) method is a very promising approach for the simulation of turbulent flows because computation times are significantly lower than those needed for DNS. Moreover, their resolution of turbulent structures is more accurate in comparison to RANS simulations [33]. The LES method is commonly used in the study of turbulent flows in which large scales of motion are resolved and the effect of small scales is modeled with the help of a sub-grid scale (SGS) model which usually employs an eddy viscosity assumption to model the SGS stress.

In the present work, the Wall-Adapting Local Eddy-Viscosity (WALE) model was used because it overcomes the limitations of the Smagorinsky model [41]. The WALE model uses a specific velocity scale for the calculation of eddy viscosity which enables it to predict accurate values in the regions of high vorticity as well as high irrotational strain [43]. The governing equations can be summarized as follows.

The instantaneous local variable is divided, based on the filter, to resolvable scale variable $\bar{\varphi}_i$, and subgrid-scale one $\acute{\varphi}_i$,

$$\varphi_i = \bar{\varphi}_i + \acute{\varphi}_i. \tag{1}$$

The filtered equations are developed from the incompressible Navier-Stokes equations of motion,

$$\frac{\partial u_i}{\partial t} + u_j \frac{\partial u_i}{\partial x_j} = -\frac{1}{\rho}\frac{\partial p}{\partial x_i} + \frac{\partial}{\partial x_j}\left(\upsilon \frac{\partial u_i}{\partial x_j}\right). \tag{2}$$

Where the u_i, p, and υ are the i-th velocity component, pressure and kinematic viscosity of fluid flow, respectively. Using the decomposition of Eq. (1) for velocity and pressure, then filtering Eq. (2) gives the equations of motion for the resolved flow field as follows,

$$\frac{\partial \bar{u}_i}{\partial t} + \bar{u}_j \frac{\partial \bar{u}_i}{\partial x_j} = -\frac{1}{\rho}\frac{\partial \bar{p}}{\partial x_i} + \frac{\partial}{\partial x_j}\left(\upsilon \frac{\partial \bar{u}_i}{\partial x_j}\right) + \frac{1}{\rho}\frac{\partial \tau_{ij}}{\partial x_i}. \tag{3}$$

The extra term $\frac{\partial \tau_{ij}}{\partial x_i}$ in Eq. (3) represents the divergence of SGS stress tensor, arises from the non-linear advection terms, due to the fact that

$$\overline{u_j \frac{\partial \bar{u}_i}{\partial x_j}} \neq \bar{u}_j \frac{\partial \bar{u}_i}{\partial x_j}, \tag{4}$$

hence the SGS stress tensor,

$$\tau_{ij} = \overline{u_i u_j} - \bar{u}_i \bar{u}_j. \tag{5}$$

Similar equations can be derived for the subgrid-scale field. Subgrid-scale turbulence models usually seek to calculate the SGS stress using the following assumption,

$$\tau_{ij} - \frac{1}{3}\tau_{kk}\delta_{ij} = -2\rho \upsilon_t \bar{S}_{ij}. \tag{6}$$

The isotropic part of the subgrid-scale stresses τ_{kk} is not modeled but added to the filtered static pressure term. $\bar{S}_{ij}$ is the rate-of-strain tensor for the resolved scale defined by

$$\bar{S}_{ij} = \frac{1}{2}\left(\frac{\partial \bar{u}_i}{\partial x_j} + \frac{\partial \bar{u}_j}{\partial x_i}\right), \tag{7}$$

and υ_t is the kinematic turbulence viscosity. Substituting into the filtered Navier-Stokes equations Eq. (3),

$$\frac{\partial \bar{u}_i}{\partial t} + \bar{u}_j \frac{\partial \bar{u}_i}{\partial x_j} = -\frac{1}{\rho}\frac{\partial \bar{p}}{\partial x_i} + \frac{\partial}{\partial x_j}\left([\upsilon + \upsilon_t]\frac{\partial \bar{u}_i}{\partial x_j}\right), \tag{8}$$

In these equations (Eqs. (2) – (8)), the incompressibility constraint has been used to simplify the equation. Then the pressure is modified to include the trace term $\tau_{kk}\delta_{ij}/3$, where the δ_{ij} is the Kronecker delta. In the WALE model the eddy viscosity is calculated by

$$\mu_t = \rho L_S^2 \frac{(S_{ij}^d S_{ij}^d)^{3/2}}{(\bar{S}_{ij}\bar{S}_{ij})^{5/2}+(S_{ij}^d S_{ij}^d)^{5/4}}. \quad (9)$$

where,

$$L_s = C_w V^{1/3}, \quad (10)$$

$$S_{ij}^d = \frac{1}{2}\left(\bar{g}_{ij}^2 + \bar{g}_{ji}^2\right) - \frac{1}{3}\delta_{ij}\bar{g}_{kk}^2, \quad (11)$$

$$\bar{g}_{ij} = \frac{\partial \bar{u}_i}{\partial x_j}, \quad (12)$$

$$\bar{g}_{ij}^2 = \bar{g}_{ik}\bar{g}_{kj} \quad (13)$$

where, the constant $C_w = 0.325$, and V is the volume of the computational cell.

3. Numerical Settings

The employed geometry, meshing, boundary conditions, and solvers are discussed in detail in this section. Where the work here is divided into two parts; first one is the validation and mesh dependency test, while the second part contains a parametric study. In the second part, the impact of the jet exit velocity will be analyzed.

3.1. Geometry and Meshing

In this work, 2-dimensional simulations were performed in a rectangular domain with dimensions of 40D x 13D, where D is the jet diameter as it illustrated in the schematic diagram in Fig. 1. The boundary condition: as it is shown in Fig. 1, (velocity inlet) at the edges number 1 and 2, and (pressure outlet) at edges number 3 and 4. First of all, the employed model and domain are validated with the work of Pavlović et al. [44]. The validation was performed by comparing the current work at four different mesh size with that of Pavlović et al. [44]. The four cases M1, M2, M3, and M4 are summarized in Table 1.

Table 1: Mesh specifications

	M1	M2	M3	M4
Element size	D/10	D/13	D/30	D/50
Number of elements N=($N_y \times N_x$)	130 x 400 = 52,000	169 x 520 = 87,880	390 x 1200 = 468,000	650 x 2000 = 1,300,000

The mesh is a structured equidistance quad-cells with cell size of D/10, D/13, D/30 and D/50, leads to total number of elements of 52 000, 87 880, 468 000, 1 300 000 for Cases M1, M2, M3, and M4, respectively. Where the diameter of the jet in these cases is 0.1 mm.

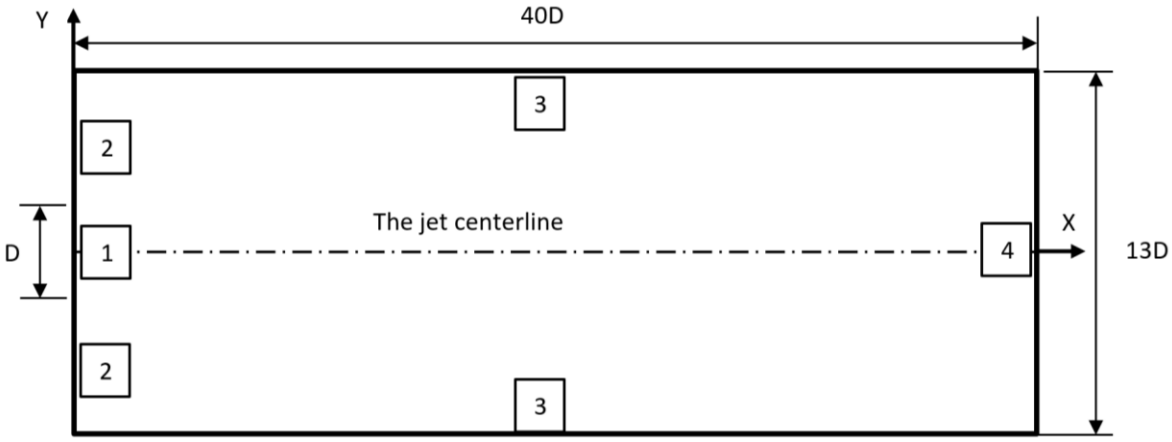

Figure 1: Schematic diagram shows the dimensions of the computational flow domain and boundary conditions

3.2. Numerical Setups and Models

The properties of the liquid jet and the surrounding gas of fluids used in the study (validation and present cases) are listed in Table 2. Ansys-Fluent 19.R3 was used in this work for all simulations with the following settings. Volume of fluid (VOF) was used as a multiphase model for its convenience with the free jet flows. LES with WALE Subgrid-scale model was used as a turbulence model. Liquid diesel for the jet and air for surrounding gas were used as working fluids. The time step size in the range from 1×10^{-8} s to 3×10^{-8} s was used in the simulations, ensuring maximum Courant–Friedrichs–Lewy condition (CFL) of 0.9.

3.3. Mesh Dependency and Validation

Mesh dependency test has been performed by using four mesh resolution levels as described in Sec. 3.1; from coarse to fine. Conditions similar to that of Pavlović et al. [44] selected in the validation and mesh dependency stage are summarized in Table 2. Figure 2 shows the jet structure of the liquid jet at time $t= 6\ \mu$s that was obtained from the simulation using different mesh sizes (M1, M2, M3, and M4) and compared with reference case from Ref. [44]. As it can be observed from Fig. 2, the jet structure at Case M1, is completely different than that from the reference case. It is very obvious that the large cell size is not enough to capture the liquid breakup and shear layer in appropriate manner. With decreasing the cell size, the jet structure approaches that of the reference case, especially for Cases M3 and M4.

This can be confirmed more precisely from computing the liquid core length, according to the definition of Pavlović et al. [44], at different jet exit velocity. The liquid core is defined, here, as the region where the mean liquid volume fraction is greater than 0.5. The computed liquid core length at jet exit velocities of 50 m/s, 100, m/s and 150 m/s for the different mesh sizes and the reference case is shown in Fig. 3. M1 and M2 give farther values of potential core length, from the reference case, than M3 and M4 with maximum percentage errors of 39.5%, 23.7%, 4.9% and 2.6%, respectively.

Table 2: Initial conditions used for the validation case and the parametric study part

	Validation part	**Present study**
Diameter, D, [mm]	0.1	0.05
Exit jet velocity, U_e, [m/s]	50, 100, 150	50, 100, 150
Liquid density, ρ_l, [kg/m^3]	810.5	810.5
Liquid dynamic viscosity, μ_l, [kg/m.s]	1.54×10^{-3}	1.54×10^{-3}
Surface tension, σ, [N/m]	0.0264	0.0264
Liq. Weber Number, $We_l = \frac{\rho_l {U_r}^2 D}{\sigma}$	7675, 30701, 69077	3838, 15350, 34538
Reynolds number, Re $= \frac{\rho_l U_e D}{\mu_l}$	2631, 5263, 7894	1316, 2631, 3947
Turbulence intensity $[I] = 0.16\mathrm{Re}^{-1/8}$ [%] [40]	5.98, 5.48, 5.21	6.5, 6, 5.7
Gas density, ρ_g [kg/m^3]	34.5	34.5
Gas dynamic viscosity, μ_g, [kg/m.s]	1.54×10^{-5}	1.54×10^{-5}
Gas Weber Number, $We_g = \frac{\rho_g {U_r}^2 D}{\sigma}$	327, 1307, 2940	163, 653, 1470

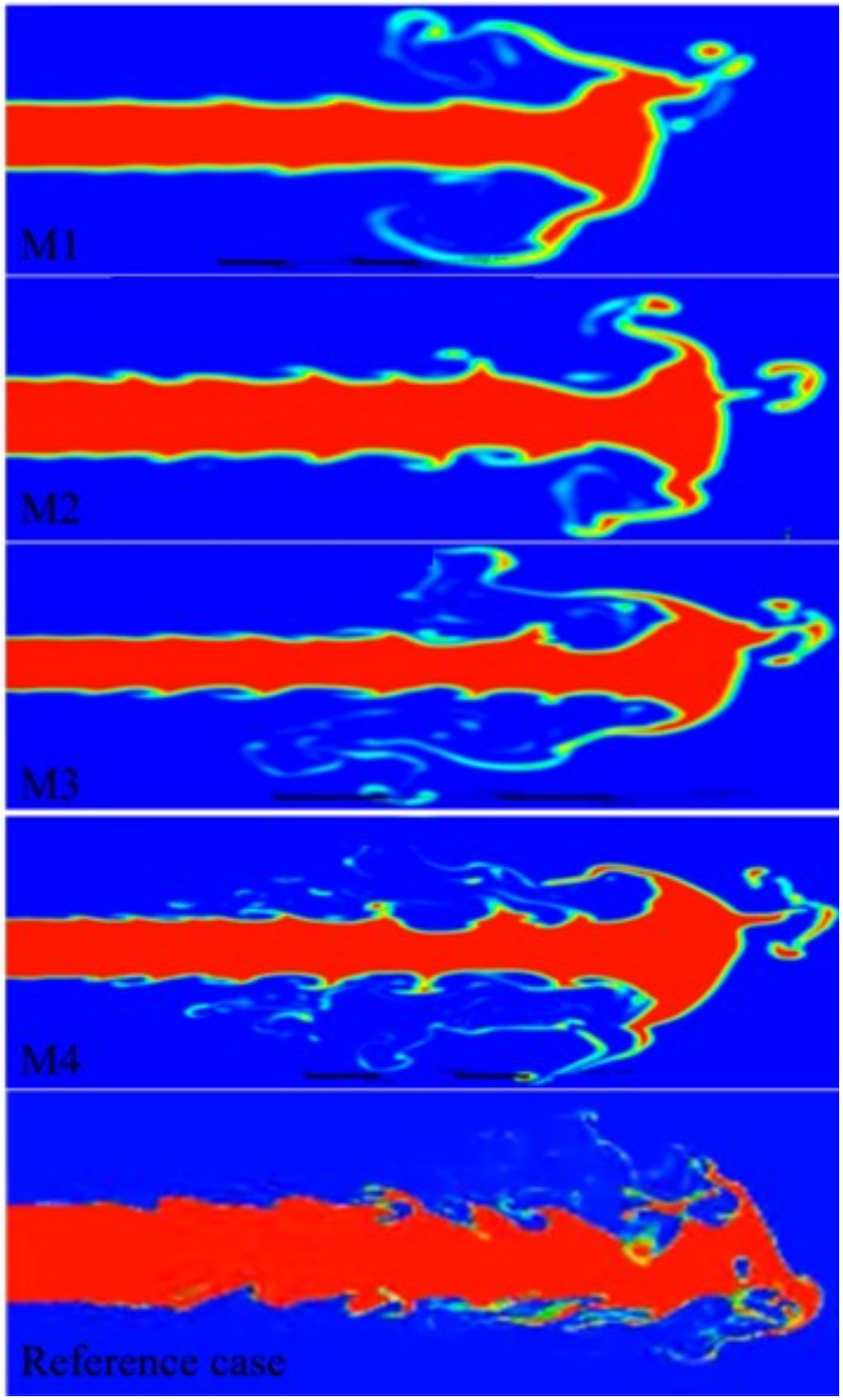

Figure 2: Volume fraction of the liquid jet at time of 6 μs at jet velocity of 100 m/s. The cases from top to bottom are M1, M2, M3, M4, and reference case from by Pavlović et al. [44].

With these results, it can be concluded that the used computational model is able to simulate the jet breakup and give results with acceptable errors (as in M3 and M4).

To compromise between the available resources and the accuracy of the computational simulation, it was decided that the cell size of the case M3 will be employed in the rest of this work.

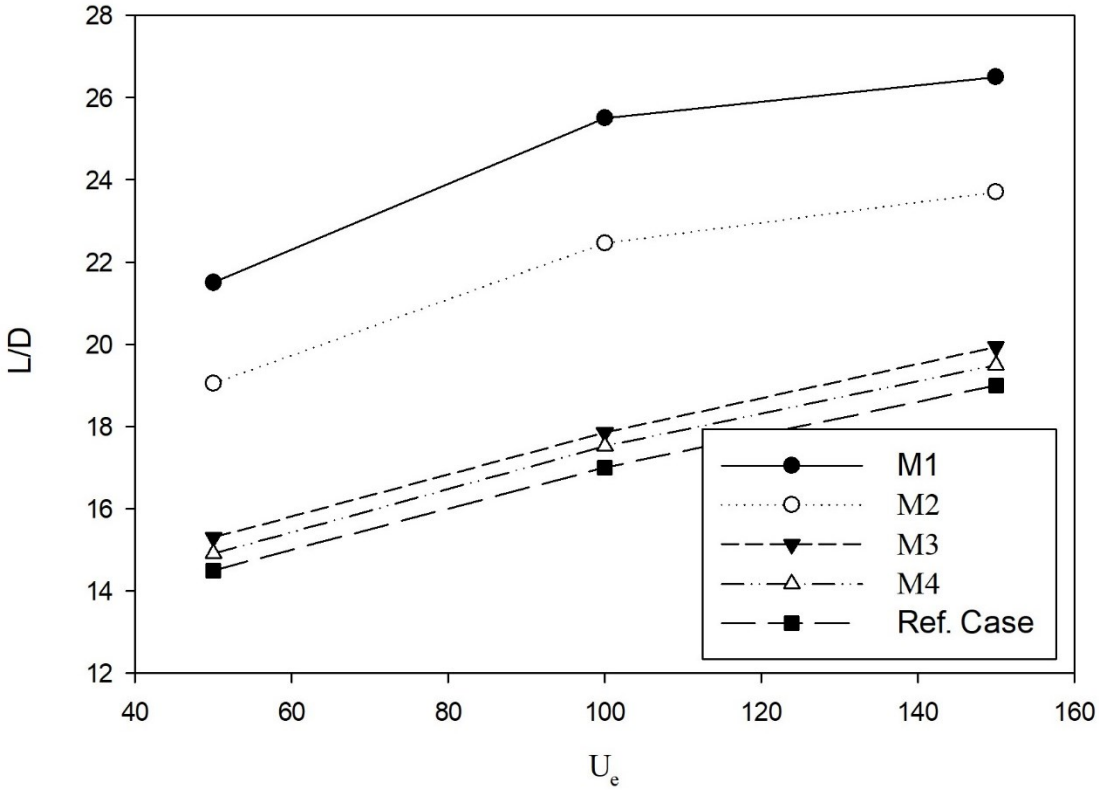

Figure 3: Liquid core length obtained from the present simulation at different cell size (M1, M2, M3, and M4) and the result of Pavlovic et al. [44] with different jet injection velocities (50, 100, 150 m/s).

4. Results and Discussion

After validating the employed models and finishing the mesh dependency test, the impact of changing the jet velocity on the turbulent jet behavior will be investigated. Three different velocities will be investigated U_e= 50, 100, 150 m/s, which are named hereinafter Case50, Case100, and Case150 respectively.

4.1. Liquid jet structure

Fig. 4 compares the liquid jet structures predicted for different exit jet velocities at non-dimensional time $T = 5$. The time is non-dimensionalized by the flow through time, $T = \frac{real\ time}{flow\ throug\ time}$ as it recommended by references. [36] and [37]. The flow through time = L/U_e, where L is the length of the computational domain in the flow direction. As it can be observed from Fig. 4, the morphologies of the liquid jet breakup process are well produced by the current

method. It is obvious that as the jet velocity increases, the predicted location where the first drops and ligaments are seen moves away from the nozzle. This location was located at Fig. 4 at $S_1 = 3.5D, 6.5D \; and \; 7.5D$ for Case50, Case100 and Case150, respectively. This may be due to the increasing the inertia forces which comes from the momentum of the incoming jet that retard the breakup.

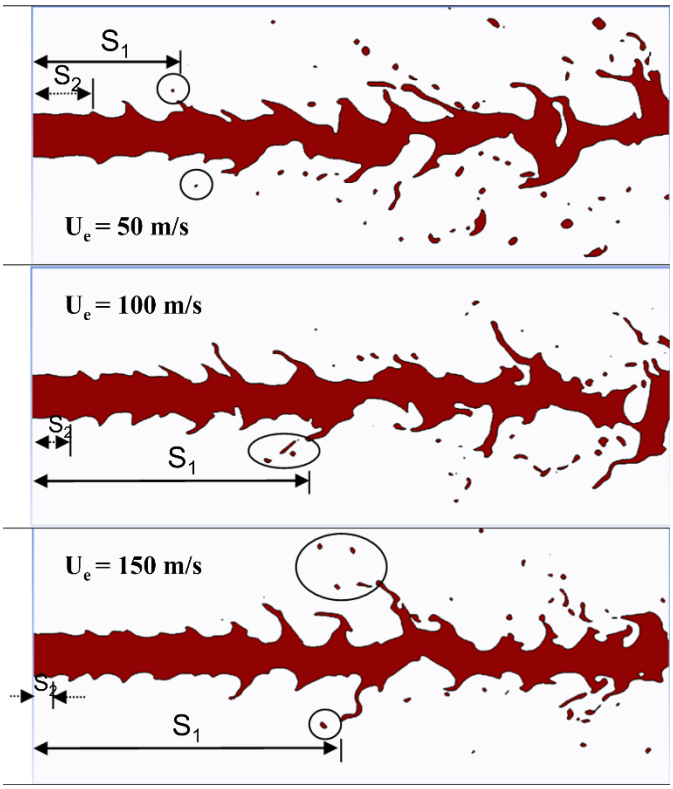

Figure 4: liquid jet structure in a part of the domain ($9D \times 15D$=, at time $T = 5$, from $X = 0$ to $15D$. **Top**: 50 m/s; **Middle**:100 m/s; **Bottom**: 150 m/s

Also, it is clear that the predicted location, where surface waves developed from Kelvin-Helmholtz instability are first seen, moves towards the nozzle as the jet velocity increases. This location was computed at $S_2 = 1.6D, 1D \; and \; 0.5D$ for Case50, Case100 and Case150. This may be due to increasing the shear stress at the interface as a result of increasing the liquid-gas relative velocity at the interface and due to increasing the turbulence inside the jet which make the disturbing liquid eddies become more energetic as the Reynolds number of the liquid flow increases from 5263 to 10526. The Kelvin–Helmholtz instability [45], [46] occurs when there is both a density gradient and a sufficiently large velocity gradient within a fluid. The structures that develop from the Kelvin–Helmholtz instability, which may rapidly become turbulent, play a crucial role in the transfer of energy from larger to smaller scales. The physical source of the instability is the underlying shear flow and its kinetic energy.

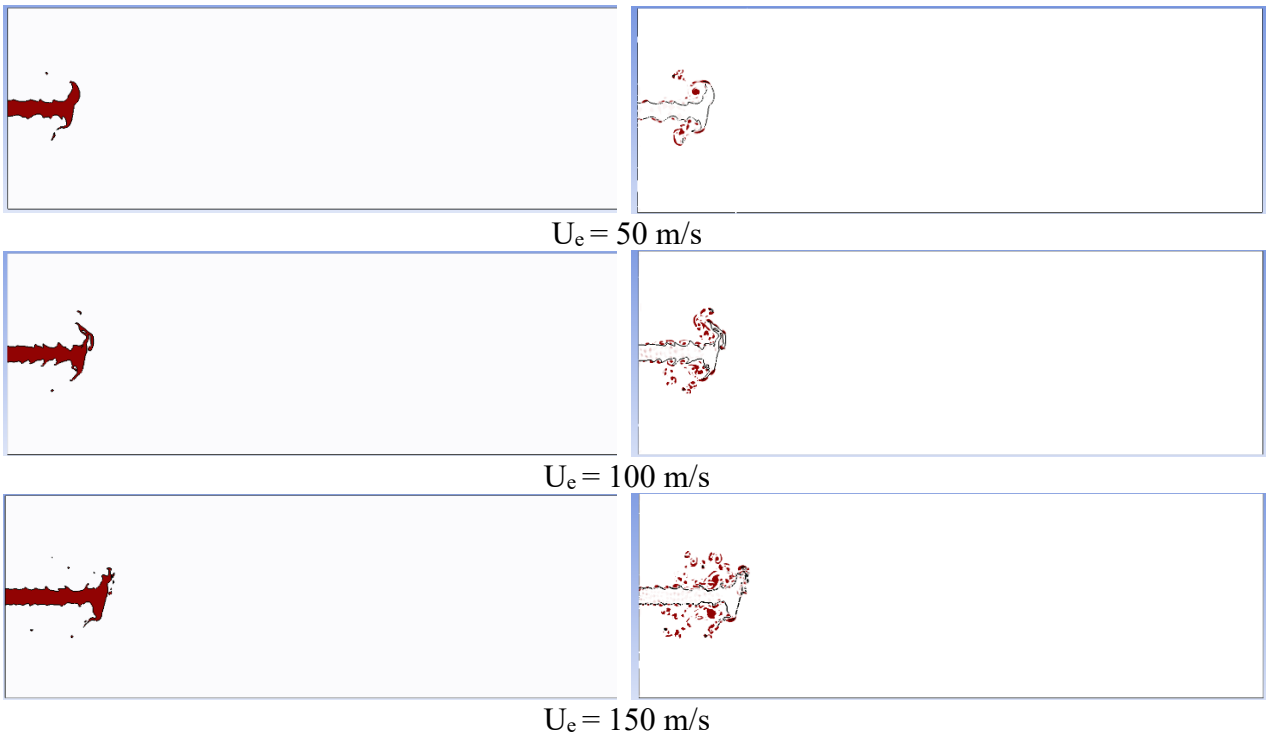

Figure 5.a: The liquid volume fraction field (left) and the Q-criteria value field (right) during earlier stage of the three liquid jet flows of velocities, 50m/s, 100m/s and 150m/s, from top to bottom.

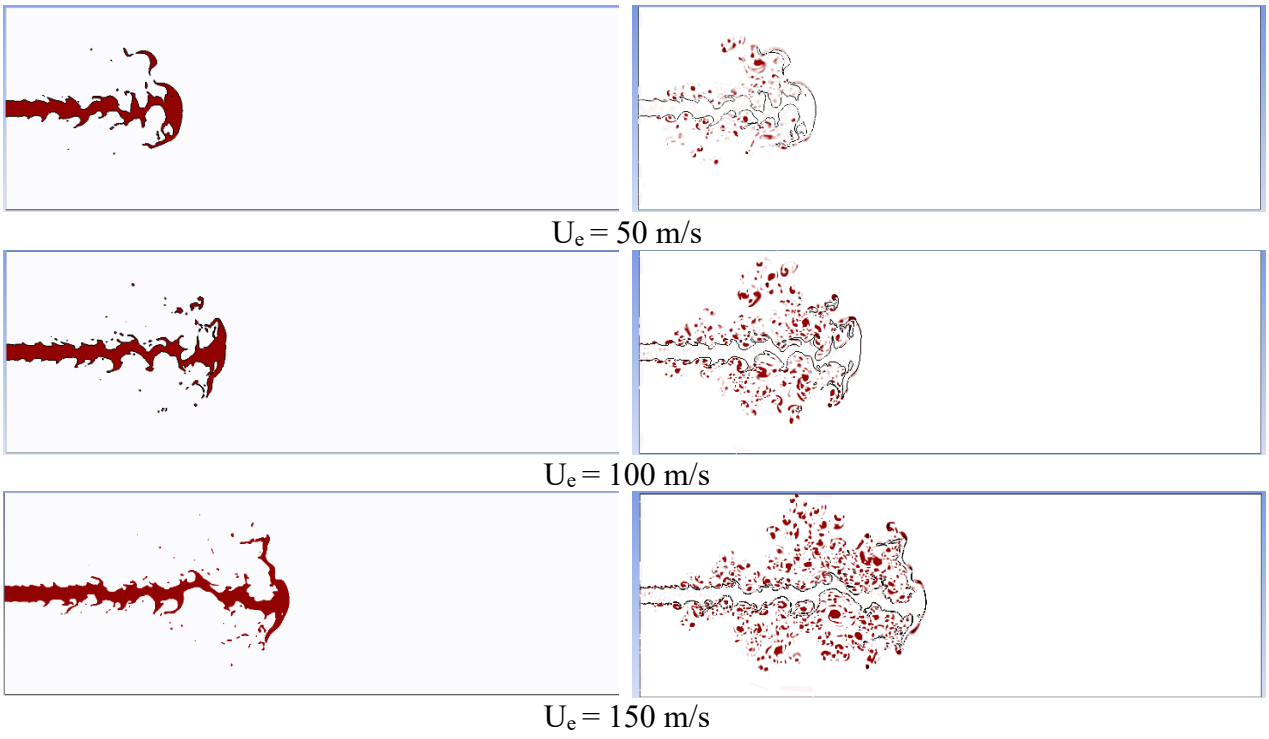

Figure 5.b: The liquid volume fraction field (left) and the Q-criteria field (right) during developing stage of the three liquid jet flows of velocities, 50m/s, 100m/s and 150m/s, from top to bottom.

4.2. Atomization in liquid jet flows

According to the values of Reynolds number of the three studied cases (Case50, Case100, and Case150), they lies in Rayleigh breakup regime. The atomization in liquid jet flows in this regime can be divided into four stages: the earlier stage of the jet, the developing stage, the breakup stage and the fully developed stage [47].

In Fig. 5, the liquid volume fraction field (left) and the Q-criteria field (right) during four stages of the liquid jet flow are shown. Fig. 5.a (left) shows the volume fraction field of the liquid in the earlier stage of the jet. In this stage, the umbrella shape appears in the head area of the jet due to the influence of the air motion. Driven by the vortex near the jet head, the liquid begins to move toward outsides, and the tip appears. According to Plateau-Rayleigh instability, the tip will break up to ligaments and tiny droplets driven by the surface tension. The Plateau–Rayleigh instability [48], [46] is a surface-tension driven instability, which occurs when a column or stream of liquid breaks up into smaller drops, which have less total surface area. With smaller liquid volumes (not dominated by gravity), surface tension favors drop-like shapes since, for an isolated free liquid of constant volume, the minimal surface is obtained for a sphere.

Figure 5.a (right) shows the Q-criteria field of the liquid in the earlier stage of the jet. The Q-criterion is plotted to visualize the vortical structures. The Q-criterion is defined as,

$$\mathrm{Q} = 0.5(\|\Omega\|^2 - \|S\|^2)$$

where, Ω is the rotation rate or vorticity tensor and S is the strain rate tensor. From this we can see that positive values of Q are indicative of areas in the flow field where the vorticity dominates and negative values of Q are indicative of strain rate or viscous stress dominated areas. Here, the positive values were just displayed in the figure shown. There are some vortexes under the umbrella. In this region, tiny droplets interact with the air motion. According to Salvador et al. [49], vortices will help the primary breakup. The schematic of the flow field in the earlier stage of the jet is shown in Fig. 5a. The calculations showed that the earlier stage of the lower exit velocity jet occurs before that of the jet has higher exit velocity. The normalized times at which the earlier stage occurred were T= 0.14, 0.16 and 0.2 for Case50, Case100 and Case150, respectively.

The developing stage and the breakup stage are shown in Fig. 5.b and Fig. 5.c, respectively. At the development stage, the head of the jet is still similar to an umbrella, but the shape is deformed. In Fig. 5.b, the waves at the gas-liquid interface, due to the Kelvin–Helmholtz instability mechanism, are no longer small. In the correct sense, it is no longer the only one visible on the surface; where large amplitude wave fluctuations also appeared downstream it. This developing stage also occurred earlier with the jet of lower exit velocity, where it occurred in the jets of Case50, Case100 and Case150 at normalized times of T=0.36, 0.45 and 0.58.

In the breakup stage, the growing wave fluctuation propagates along the liquid jet, and the head of the jet begins to break up. The symmetry breaking occurs during this stage. The liquid part in the breakup zone will further deform, and larger pieces of the liquid will break up to smaller pieces due to the stretching effect of the turbulent flow. This shows that the Kelvin-Helmholtz instability mechanism dominates the breakup stage. This breakup stage, in the jets of 50m/s, 100m/s and 150m/s exit velocities, occurs at normalized times of T= 0.5, 0.54 and 0.71.

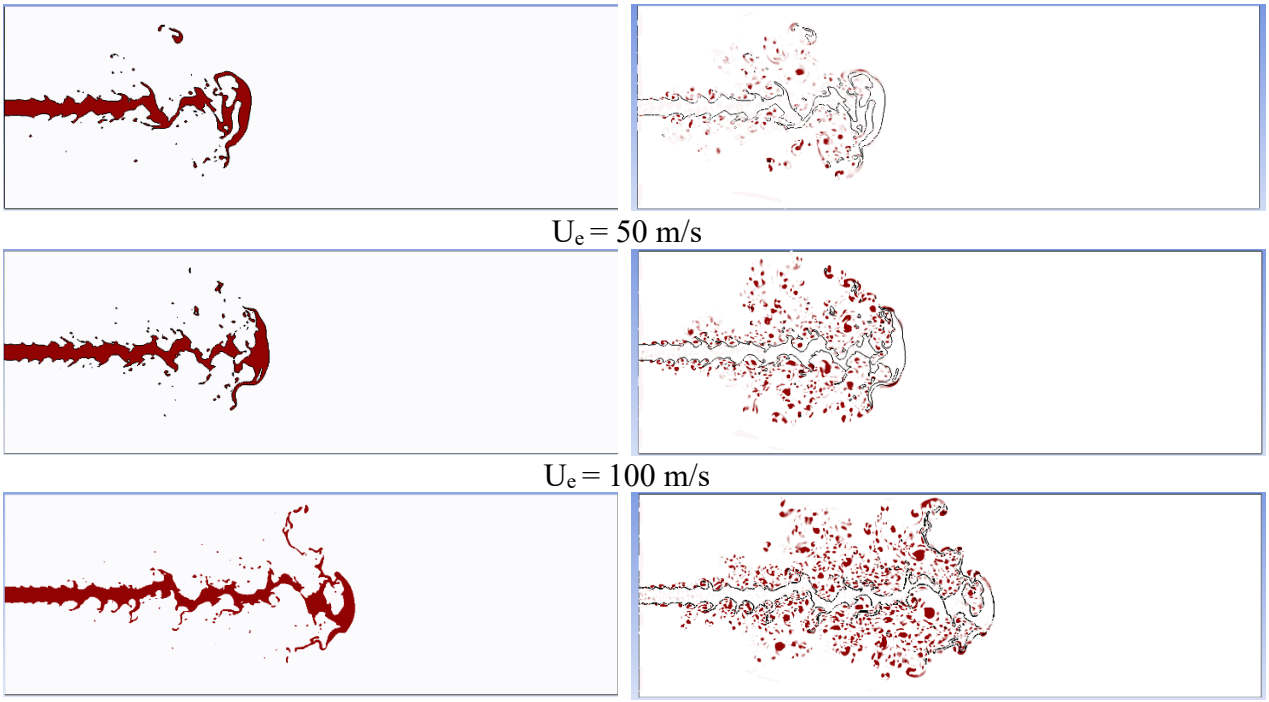

Figure 5.c: The liquid volume fraction field (left) and the Q-criteria value field (right) during breakup stage of the three liquid jet flows of velocities, 50m/s, 100m/s and 150m/s, from top to bottom.

4.3. Turbulent kinetic energy

Figure 6 shows the contours of normalized turbulence kinetic energy (TKE) of the jet with the three velocities at normalized $T = 5.25$. The normalized TKE was computed to be nearly zero inside the laminar potential core and outside the jet. The region having normalized TKE less than 5% of the maximum value was considered the laminar zone. The maximum normalized TKE in the three cases equals 0.1, then the contour of 5% has value of 0.005. The contour of normalized TKE of 0.005 considered to separate the laminar region from the turbulent region of the jet was colored black in Fig. 6.

It is shown in the figure that the high TKE near the shear layer merged closer to the nozzle exit at the centerline (Fig. 6) due to shorter potential core length for all case. However, the region of higher values of normalized TKE (that starts from 0.06 to above and colored with yellow to red) increased with increasing of the jet velocity.

4.4. Average contours

The time-average liquid volume fraction (ALVF) contours are presented in Fig. 7. The overall sight of the dispersion intensity of disintegrated ligaments and droplets from the jet surface, represented in the prevalence of contour line of 0.05 ALVF in the domain [50], [51], can be noted from Fig. 7. It is found that the dispersion increases with increasing the jet exit velocity, where the radius of expansion in radial direction of the ALVF contour of 0.05 is $2.35D$, $2.65D$ and $3.15D$ for Case50, Case100 and Case150, respectively. This can be discussed in terms of

spray dispersion angles 6.88°, 7.66° and 9.4°, respectively, as it will be confirmed in the next section.

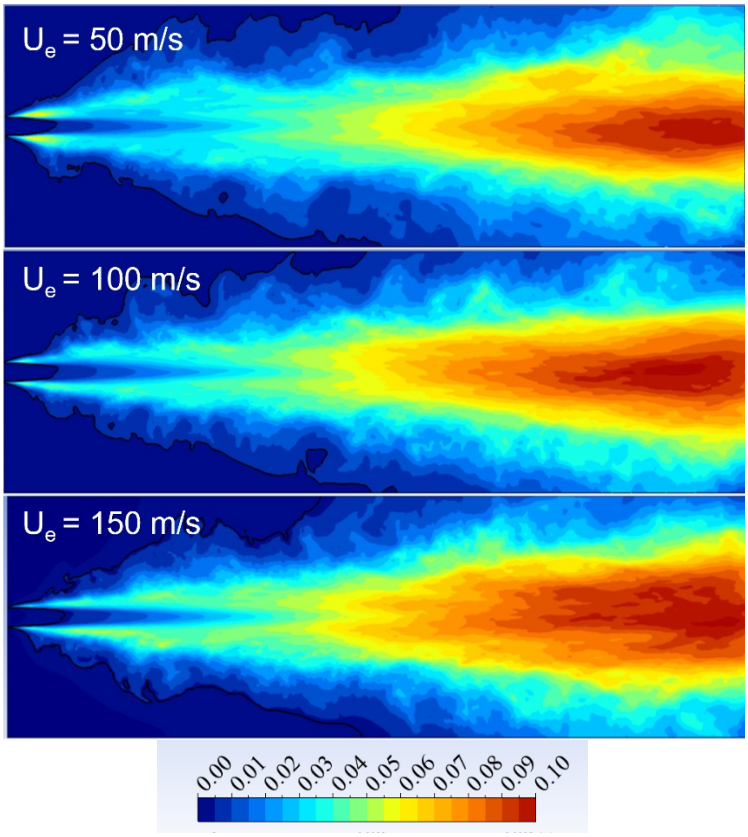

Figure 6: Instantaneous normalized TKE, at normalized time $T = 5.25$, for Case50, Case100 and Case150 from top to bottom.

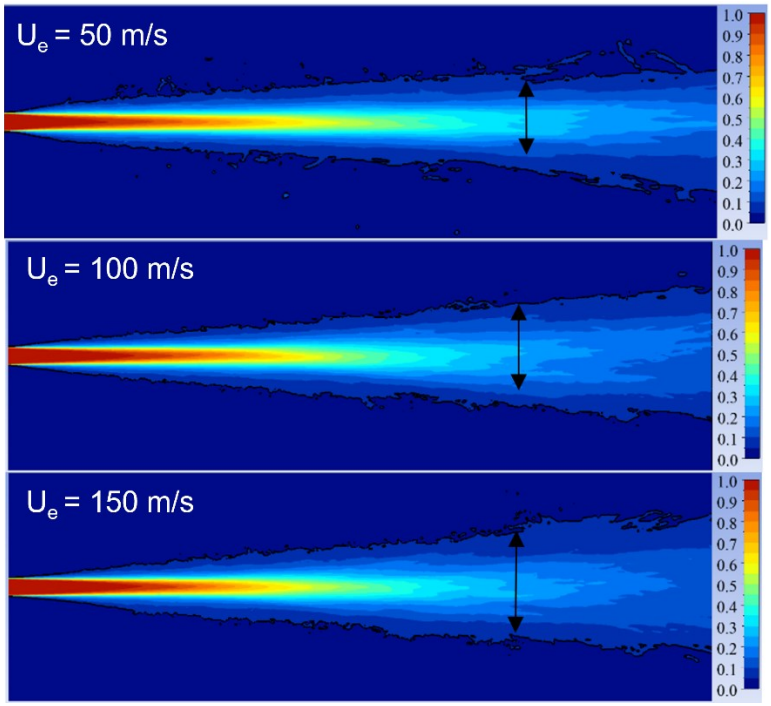

Figure 7: Contours of time-averaged liquid volume fraction at $T = 5.25$, for Case50, Case100 and Case150 from top to bottom

4.5. Centerline average values

Comparing the decay of the normalized centerline axial velocity, u_{avg}/U_e (where u_{avg} is local centerline velocity along the jet direction and U_e is the velocity at the orifice) of the three jets with each other, the three cases show little differences as shown in Fig. 8 (left). The centerline velocity wasn't kept after issuing from the orifice in all the three cases. The end of the potential core is defined where the centerline velocity decreased to 95% of the centerline velocity at the orifice according to [52]. Based on this criterion, the potential core length was computed to be about 10D with all cases (which is also clear from the velocity contours in Fig. 7). Thus, the decay of centerline averaged velocity indicates a low sensitivity of the potential core length to the range of studied conditions. However, the average liquid volume fraction, shown in Fig. 8 (right) predicts larger potential core length of $10D$ for the larger exit velocity (Case150), whereas it equals $9.75D$ and $9.25D$ for Case100 and Case50, respectively.

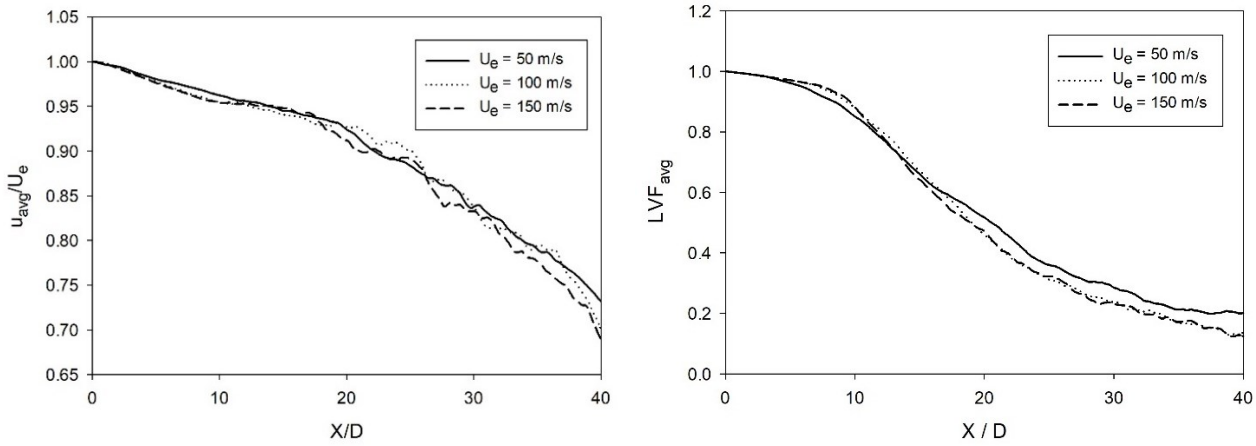

Figure 8: Centerline cut of temporal-average of streamwise velocity (left), and liquid volume fraction (right).

Beyond the potential core, the normalized centerline velocity for all cases decreased with moderate rate to $x = 18D$ (0.07 through $18D$), then the rate of decrease became faster (i.e. with a steeper slope) to the end of domain (0.23 through $22D$). On the other hand, at $x = 40D$, the LVF in Case50 reached 0.2, whereas Case100 and Case150 reaches 0.12, which means that the dispersion of the jet and its mixing with the surrounding fluid is faster in jets with higher exit velocity, that agrees the analysis of previous section.

4.6. Radial Profiles at X-Distances from the Jet Exit

Figure 9 shows radial profiles of the normalized average streamwise velocity downstream locations of $5D$, $15D$, $25D$, and $35D$ from the jet exit. At $x = 5D$, the velocity profiles, for the three cases, followed a similar path having a maximum radius of expansion in radial direction of $3D$, beyond which the axial velocity became almost zero. It was observed that the maximum velocity located at $y = \pm 0.6D$ not at the centerline. At $x = 15D$, the velocity profiles also followed a similar path, however it expanded more in the radial direction having a maximum radius of $6D$. The maximum velocity still observed at $y = \pm 0.6D$ with a value of $0.9U_e$. At $x = 25D$, the maximum axial velocity was observed at the jet centerline with a smaller normalized value of 0.74 as compared to that at $x = 5D$ and $x = 15D$. The jet velocity profiles expanded more in the radial direction with different radii for each case. Case150 had the most expanded profile to $y = \pm 4.5D$ and Case50 had the least, then all of them reaches zero axial velocity at $y = 6.5D$. At $x = 35D$, the velocity profile showed a bill shape peak at the jet center with a normalized velocity magnitude of 0.6 and decreased to 0.05 at $y = 6.5D$ for all cases. The velocity was above zero in a larger radial space as compared to prior cases.

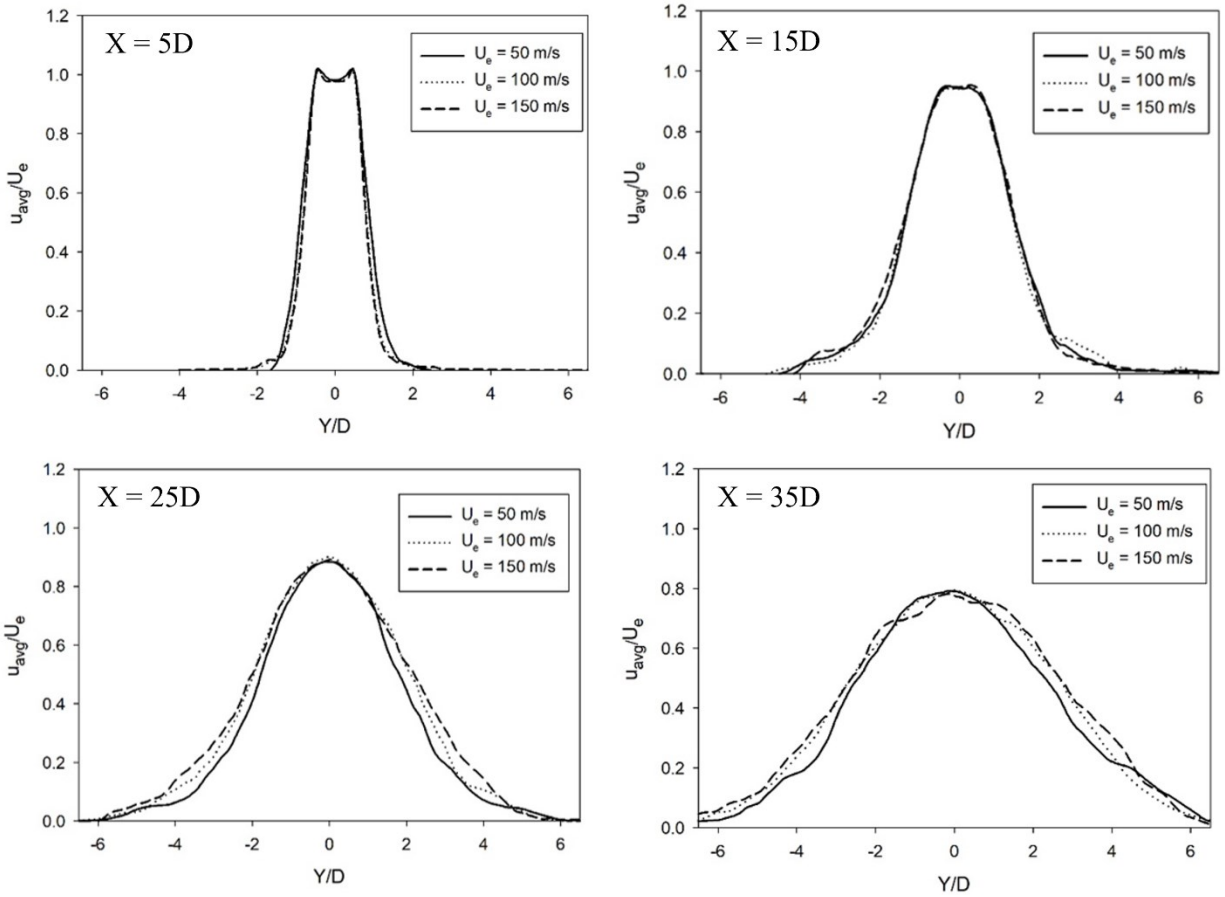

Figure 9: Time-averaged normalized axial velocity at different x-locations

5. Conclusion

In this work, the impact of the jet exit velocity on the characteristics of the turbulent liquid jet is investigated numerically using LES in ANSYS-FLENT. Validation and grid independency test first performed at different jet velocities. Then the impact of the jet exit velocity is investigated by changing the value of $U_e = 50\ m/s$ (Case50), $U_e = 100\ m/s$ (Case100)and $U_e = 150\ m/s$ (Case150.) It can be concluded that,

- The predicted location, where drops and ligaments are first seen, moves away from the nozzle as the jet velocity increases. This location was computed at $x = 3.5D, 6.5D$ and $7.5D$ for Case50, Case100 and Case150, respectively.
- The predicted location, where surface waves developed from Kelvin-Helmholtz instability are first seen, moves towards the nozzle as the jet velocity increases. This location was computed at $x = 1.6D, 1D\ and\ 0.5D$ for Case50, Case100 and Case150, respectively.
- The occurrence time of any of the four atomization stages of the jet is directly proportional to the jet exit velocity, where the normalized times at which
    - the earlier stage occurred were 0.14, 0.16 and 0.2 for Case50, Case100 and Case150, respectively.

  - the developing stage occurred were 0.36, 0.45 and 0.58 for Case50, Case100 and Case150, respectively.
  - the breakup stage occurred were 0.5, 0.54 and 0.71 for Case50, Case100 and Case150, respectively
- The region of higher values of turbulent kinetic energy TKE increased with increasing of the jet velocity.
- The jet dispersion angle increases with increasing the jet exit velocity, where it was calculated as 6.88°, 7.66° and 9.4°, for Case50, Case100 and Case150, respectively.
- The decay of centerline averaged velocity indicates a low sensitivity of the potential core length to the range of studied conditions. However, the average liquid volume fraction predicts larger potential core length of $10D$ for the larger exit velocity (Case150), whereas it equals $9.75D$ and $9.25D$ for Case100 and Case50, respectively.
- At $x = 25D$, Case150 has the most expanded radial profile of axial velocity to $y = \pm 4.5D$ and Case50 had the least, then all of them reaches zero axial velocity at $y = 6.5D$.

In the future, it is intended to conduct further investigations for more jet exit-velocity values out of the range investigated here, in order to get deeper understand the relationship between exit velocity and spray properties.

Compliance with Ethical Standards

All authors declare that the current work follows the ethical standards, where it is not associated with any conflict of interest. This work has been done without any external or internal funding. All the authors have an essential contribution.

REFERENCES

[1] N. Ashgriz, *Atomization Hand Book*. 2011.

[2] M. R. Morad, M. Nasiri, and G. Amini, “Axis-switching and breakup of rectangular liquid jets,” *Int. J. Multiph. Flow*, vol. 126, p. 103242, 2020, doi: 10.1016/j.ijmultiphaseflow.2020.103242.

[3] N. Odier, G. Balarac, and C. Corre, “Numerical analysis of the flapping mechanism for a two-phase coaxial jet,” *Int. J. Multiph. Flow*, vol. 106, pp. 164–178, 2018, doi: 10.1016/j.ijmultiphaseflow.2018.05.028.

[4] H. Eroglu and N. Chigier, “WAVE CHARACTERISTICS OF LIQUID JETS FROM AIRBLAST COAXIAL ATOMIZERS,” *At. Sprays*, vol. 1, no. 4, pp. 349–366, 1991, doi: 10.1615/AtomizSpr.v1.i4.10.

[5] F. Savart, “Mémoire sur la constitution des veines liquides lancées par des orifices circulaires en mince paroi,” *Ann. Chim.*, vol. 53, pp. 98–337, 1833.

[6] M. J. McCarthy and N. A. Molloy, “Review of stability of liquid jets and the influence of nozzle design,” *Chem. Eng. J.*, vol. 7, no. 1, pp. 1–20, 1974, doi: 10.1016/0300-9467(74)80021-3.

[7] A. H. Lefebvre and V. G. McDonell, *Atomization and Sprays*. Second edition. | Boca Raton : Taylor & Francis, CRC Press, 2017.: CRC Press, 2017. doi: 10.1201/9781315120911.
[8] "Regimes of Jet Breakup and Breakup Mechanisms (Physical Aspects)," in *Recent Advances in Spray Combustion: Spray Atomization and Drop Burning Phenomena*, Washington DC: American Institute of Aeronautics and Astronautics, 1996, pp. 109–135. doi: 10.2514/5.9781600866418.0109.0135.
[9] S. P. Lin and R. D. Reitz, "Drop and spray formation from a liquid jet," *Annu. Rev. Fluid Mech.*, vol. 30, pp. 85–105, 1998, doi: 10.1146/annurev.fluid.30.1.85.
[10] C. Dumouchel, "On the experimental investigation on primary atomization of liquid streams," *Exp. Fluids*, vol. 45, no. 3, pp. 371–422, 2008, doi: 10.1007/s00348-008-0526-0.
[11] H. Hiroyasu and T. Kadota, "Fuel droplet size distribution in diesel combustion chamber," *SAE Tech. Pap.*, vol. 83, pp. 2615–2624, 1974, doi: 10.4271/740715.
[12] M. M. Elkotb, "Fuel atomization for spray modelling," *Prog. Energy Combust. Sci.*, vol. 8, no. 1, pp. 61–91, 1982, doi: 10.1016/0360-1285(82)90009-0.
[13] K. S. Varde, D. M. Popa, and L. K. Varde, "Spray angle and atomization in diesel sprays," *SAE Tech. Pap.*, vol. 93, pp. 779–787, 1984, doi: 10.4271/841055.
[14] G. M. Faeth, L. P. Hsiang, and P. K. Wu, "Structure and breakup properties of sprays," *Int. J. Multiph. Flow*, vol. 21, pp. 99–127, 1995, doi: 10.1016/0301-9322(95)00059-7.
[15] R. D. Reitz and F. V. Bracco, "Mechanism of atomization of a liquid jet," *Phys. Fluids*, vol. 25, no. 10, pp. 1730–1742, 1982, doi: 10.1063/1.863650.
[16] a. Fath, C. Fettes, and a. Leipertz, "Investigation of the Diesel Spray Break-Up Close to the Nozzle at Different Injection Conditions," *The Fourth International Symposium COMODIA 98*. pp. 429–434, 1998.
[17] A. Gupta, H. Guo, M. Zhai, and C. N. Markides, "Primary atomization of liquid-fuel jets in confined turbulent pipe-flows of air at elevated temperatures," *Int. J. Heat Mass Transf.*, vol. 196, p. 123285, 2022, doi: 10.1016/j.ijheatmasstransfer.2022.123285.
[18] C. Hotz, M. Haas, S. Wachter, S. Fleck, and T. Kolb, "Experimental investigation on entrainment in two-phase free jets," *Fuel*, vol. 335, no. July 2022, p. 126912, 2023, doi: 10.1016/j.fuel.2022.126912.
[19] A. Kumar and S. Sahu, "Preheated liquid jet breakup dynamics in a twin-fluid injector," *Chem. Eng. Sci.*, vol. 257, p. 117723, 2022, doi: 10.1016/j.ces.2022.117723.

[20] S. Martínez-Martínez, F. A. Sánchez-Cruz, J. M. Riesco-Ávila, A. Gallegos-Muñoz, and S. M. Aceves, "Liquid penetration length in direct diesel fuel injection," *Appl. Therm. Eng.*, vol. 28, no. 14–15, pp. 1756–1762, 2008, doi: 10.1016/j.applthermaleng.2007.11.006.

[21] H. K. Suh and C. S. Lee, "Effect of cavitation in nozzle orifice on the diesel fuel atomization characteristics," *Int. J. Heat Fluid Flow*, vol. 29, no. 4, pp. 1001–1009, 2008, doi: 10.1016/j.ijheatfluidflow.2008.03.014.

[22] W. A. Sirignano and C. Mehring, "Review of theory of distortion and disintegration of liquid streams," *Prog. Energy Combust. Sci.*, vol. 26, no. 4, pp. 609–655, 2000, doi: 10.1016/S0360-1285(00)00014-9.

[23] W. D. Bachalo, "Spray diagnostics for the twenty-first century," *At. Sprays*, vol. 10, no. 3–5, pp. 439–474, 2000, doi: 10.1615/AtomizSpr.v10.i3-5.110.

[24] D. B. Barnett, S. R. Nahorski, and E. L. Rugg, *Characteristics of (-)-[3H]-dihydroalprenolol binding to beta-adrenoceptors on rat lung membranes [proceedings]*., vol. 61, no. 3. 1977. [Online]. Available: http://www.ncbi.nlm.nih.gov/pubmed/201324%0Ahttp://www.pubmedcentral.nih.gov/articlerender.fcgi?artid=PMC1667837

[25] C. Tropea and J. Foss, "Springer Handbook of Experimental Fluid Mechanics," *Springer Handb. Exp. Fluid Mech.*, no. August 2015, 2007, doi: 10.1007/978-3-540-30299-5.

[26] N. Chigier, "The Future of Atomization and Sprays," *Proc. ILASS Eur.*, 2005.

[27] C. W. Hirt and B. D. Nichols, "Volume of fluid (VOF) method for the dynamics of free boundaries," *J. Comput. Phys.*, vol. 39, no. 1, pp. 201–225, 1981, doi: 10.1016/0021-9991(81)90145-5.

[28] S. Osher and J. A. Sethian, "Fronts propagating with curvature-dependent speed: Algorithms based on Hamilton-Jacobi formulations," *J. Comput. Phys.*, vol. 79, no. 1, pp. 12–49, 1988, doi: 10.1016/0021-9991(88)90002-2.

[29] M. Sussman and E. G. Puckett, "A Coupled Level Set and Volume-of-Fluid Method for Computing 3D and Axisymmetric Incompressible Two-Phase Flows," *J. Comput. Phys.*, vol. 162, no. 2, pp. 301–337, 2000, doi: 10.1006/jcph.2000.6537.

[30] T. Ménard, S. Tanguy, and A. Berlemont, "Coupling level set/VOF/ghost fluid methods: Validation and application to 3D simulation of the primary break-up of a liquid jet," *Int. J. Multiph. Flow*, vol. 33, no. 5, pp. 510–524, 2007, doi: 10.1016/j.ijmultiphaseflow.2006.11.001.

[31] S. Som, S. K. Aggarwal, E. M. El-Hannouny, and D. E. Longman, "Investigation of nozzle flow and cavitation characteristics in a diesel injector," *J. Eng. Gas Turbines Power*, vol. 132, no. 4, pp. 1–12, 2010, doi: 10.1115/1.3203146.

[32] W. Yuan and G. H. Schnerr, "Numerical simulation of two-phase flow in injection nozzles: Interaction of cavitation and external jet formation," *J. Fluids Eng. Trans. ASME*, vol. 125, no. 6, pp. 963–969, 2003, doi: 10.1115/1.1625687.
[33] M. Ghiji, L. Goldsworthy, P. A. Brandner, V. Garaniya, and P. Hield, "Numerical and experimental investigation of early stage diesel sprays," *Fuel*, vol. 175, pp. 274–286, 2016, doi: 10.1016/j.fuel.2016.02.040.
[34] F. Xiao, M. Dianat, and J. J. McGuirk, "LES of turbulent liquid jet primary breakup in turbulent coaxial air flow," *Int. J. Multiph. Flow*, vol. 60, pp. 103–118, 2014, doi: 10.1016/j.ijmultiphaseflow.2013.11.013.
[35] G. A. Siamas, X. Jiang, and L. C. Wrobel, "Direct numerical simulation of the near-field dynamics of annular gas-liquid two-phase jets," *Phys. Fluids*, vol. 21, no. 4, 2009, doi: 10.1063/1.3112740.
[36] H. Grosshans, A. Movaghar, L. Cao, M. Oevermann, R. Z. Szász, and L. Fuchs, "Sensitivity of VOF simulations of the liquid jet breakup to physical and numerical parameters," *Comput. Fluids*, vol. 136, pp. 312–323, 2016, doi: 10.1016/j.compfluid.2016.06.018.
[37] J. Shinjo and A. Umemura, "Simulation of liquid jet primary breakup: Dynamics of ligament and droplet formation," *Int. J. Multiph. Flow*, vol. 36, no. 7, pp. 513–532, 2010, doi: 10.1016/j.ijmultiphaseflow.2010.03.008.
[38] F. Zhang *et al.*, "Numerical simulations of air-assisted primary atomization at different air-to-liquid injection angles," *Int. J. Multiph. Flow*, vol. 158, no. November 2022, p. 104304, 2023, doi: 10.1016/j.ijmultiphaseflow.2022.104304.
[39] X. Leng *et al.*, "A numerical study on the in-nozzle cavitating flow and near-field jet breakup of a spirally grooved hole nozzle using a LES-VOF method," *Fuel*, vol. 326, no. June, p. 125016, 2022, doi: 10.1016/j.fuel.2022.125016.
[40] A. Abdelsamie and D. Thévenin, "Direct numerical simulation of spray evaporation and autoignition in a temporally-evolving jet," *Proc. Combust. Inst.*, vol. 36, no. 2, pp. 2493–2502, 2017, doi: 10.1016/j.proci.2016.06.030.
[41] R. D. C. Ward, "Monthly weather review," *Science (80-.).*, vol. 23, no. 592, pp. 714–715, 1906, doi: 10.1126/science.23.592.714.
[42] F. Nicoud and F. Ducros, "Subgrid-Scale Stress Modelling Based on the Square of the Velocity Gradient Tensor," 1999.
[43] N. Arya and A. De, "Effect of grid sensitivity on the performance of wall adapting SGS models for LES of swirling and separating–reattaching flows," *Comput. Math. with Appl.*, vol. 78, no. 6, pp. 2035–2051, 2019, doi: 10.1016/j.camwa.2019.03.038.
[44] Z. Pavlovic, S. Scheidl, W. Edelbauer, B. Basara, G. Brenn, and S. Jakirlic,

"Numerical investigation of the liquid core length in sprays with fully turbulent boundary condition," *26th Eur. Conf. Liq. At. Spray Syst. (ILASS 2014)*, no. September 2016, 2014.

[45] Helmholtz, "XLIII. On discontinuous movements of fluids," *London, Edinburgh, Dublin Philos. Mag. J. Sci.*, vol. 36, no. 244, pp. 337–346, 1868.

[46] J. Porter, P. Salgado Sánchez, V. Shevtsova, and V. Yasnou, "A review of fluid instabilities and control strategies with applications in microgravity," *Math. Model. Nat. Phenom.*, vol. 16, p. 24, Apr. 2021, doi: 10.1051/mmnp/2021020.

[47] J. Huang and X. Zhao, "Numerical simulations of atomization and evaporation in liquid jet flows," *Int. J. Multiph. Flow*, vol. 119, pp. 180–193, Oct. 2019, doi: 10.1016/j.ijmultiphaseflow.2019.07.018.

[48] J. A. F. Plateau, *Statique expérimentale et théorique des liquides soumis aux seules forces moléculaires*, no. 1873 رقم،2 مجلد. Gauthier-Villars, 1873. [Online]. Available: https://books.google.com.eg/books?id=tdf8zAEACAAJ

[49] F. J. Salvador, R. S., M. Crialesi-Esposito, and I. Blanquer, "Analysis on the effects of turbulent inflow conditions on spray primary atomization in the near-field by direct numerical simulation," *Int. J. Multiph. Flow*, vol. 102, pp. 49–63, May 2018, doi: 10.1016/j.ijmultiphaseflow.2018.01.019.

[50] V. Iyer and J. Abraham, "Penetration and dispersion of transient gas jets and sprays," *Combust. Sci. Technol.*, vol. 130, no. 1–6, pp. 315–334, 1997, doi: 10.1080/00102209708935747.

[51] Y. Jiang, Z. Issaka, H. Li, P. Tang, and C. Chen, "Range formula based on angle of dispersion and nozzle configuration from an impact sprinkler," *Int. J. Agric. Biol. Eng.*, vol. 12, no. 5, pp. 97–105, 2019, doi: 10.25165/j.ijabe.20191205.4646.

[52] S. Ashforth-Frost and K. Jambunathan, "Effect of nozzle geometry and semi-confinement on the potential core of a turbulent axisymmetric free jet," *Int. Commun. Heat Mass Transf.*, vol. 23, no. 2, pp. 155–162, Mar. 1996, doi: 10.1016/0735-1933(96)00001-2.